Regular Article

PHYSICAL CHEMISTRY RESEARCH
Published by the
Iranian Chemical Society
www.physchemres.org
info@physchemres.org

***Phys. Chem. Res.**, Vol. 3, No. 4, 265-277, December 2015.*
DOI: 10.22036/pcr.2015.10307

The Interaction of HCN Gas on the Surface of Pristine, Ga, N and GaN-Doped (4,4) Armchair Models of BPNTs: A Computational Approach

M. Rezaei-Sameti* and F. Saki

Department of Applied Chemistry, Faculty of Science, Malayer University, Malayer, 65174, Iran

(Received 27 May 2015, Accepted 28 July 2015)

In this research, the interactions of HCN gas with pristine, Ga-, N- and GaN-doped of boron phosphide nanotube (BPNTs) were investigated by using density function theory (DFT). The structure, electrical and NQR parameters, quantum descriptors involving energy gap, global hardness, global softness, electrophilicity, electronic chemical potential and electronegativity were calculated. The adsorption energy values of the AI-BIV models were negative and the adsorption process was exothermic. GaN-doped impurity atoms increased the adsorption of HCN gas on the surface of nanotube and the GaN-doped model was favorable than other models. The NQR parameters of the fourth layer of pristine and N-doped models were more than those of other models due to the change of the geometrical parameters. The energy gap between LUMO and HOMO orbital changed slightly from 2.83-3.09 eV, with adsorption of HCN gas on the surface of BPNTs. The global hardness and ionization potential and natural charge of NBO calculations showed a charge transfer from the HCN molecule (nucleophile agent) to the nanotube models (electrophile agent).

Keywords: BPNTs, DFT, HCN interaction, Ga-, N- and GaN-doped

INTRODUCTION

Hydrogen cyanide is a colorless, extremely powerful poisonous liquid that boils slightly above the room temperature. It is highly toxic by all routes of exposure and lethal to man and animals, since it inhibits the consumption of oxygen by the bodily tissue [1,2]. The amount of cyanide, the duration of exposure, and the route of exposure all influence the time to on set and the severity of illness. The medical researchers have proved that only some people are able to detect the faint and bitter odor of HCN gas and most human do not detect it, for this means HCN sensors with high sensivity are mostly appreciated [3-5]. In the recent years, monitoring of HCN gas with new sensors has become a well-established in practice [6-9]. Recently, the experimental and theoretical investigations reveal that carbon nanotube is useful to detect even small concentration of HCN gas [10-12].

*Corresponding author. E-mail: mrsameti@malayeru.ac.ir

Many research works showed that the defective single wall carbon nanotubes (SWCNTs) perform well as sensors in detecting HCN [13]. Zhang *et al*. [14] and Zhou *et al*. [15] have theoretically shown that B doped SWCNTs, Si doped boron nitride nanotubes (BNNTs) and silicium carbide nanotubes (SiCNTs) can be used as good sensors to detect HCN. Wang *et al*.'s results [16] show that the interaction of HCN with Si-doped BNNTs is associated with a remarkable charge between two fragments. In addition, Rastegar *et al*. [17], Ahmadi Peyghan *et al*. [18] and Beheshtian *et al*. [19] revealed that Al and Si doped graphenes and pristine AlNNTs are good sensitive nanotubes toward HCN molecules. Other research groups showed that doping is an appropriate method for improving the sensitivity and performance of pristine nanotubes and nano-structure materials toward HCN molecules [20-22]. In the previous research, we studied the structural, electrical and nuclear magnetic resonance parameters of AsGa, Ga, C doped on BPNTs [23-26]. In current work, DFT calculations are performed to study the effects of Ga-, N-

and GaN-doped (4,4) armchair models BPNTs on the adsorption of HCN gas. For this aim, at first step, all structures of nanotube/HCN complex at different configurations are optimized, and then, electronic structure properties, quantum parameters, adsorption energies, energy gap, net charge transfers, electronic densities of states (DOS spectrum), HOMOs and LUMOs, and NQR parameters of all representative models of BPNTs are investigated.

COMPUTATIONAL METHODS

In this work, the electronic structure properties of Hydrogen cyanide (HCN) adsorption on the surface of pristine and Ga-, N- and GaN-doped of BPNTs were investigated by using software Gaussian 03 package [27] with density functional theory (DFT) and using B3LYP functional with 6-31G (d) basis set. To study the structural parameters and electrical properties of adsorption HCN on pristine, Ga-, N- and GaN-doped on the surface of BPNTs, eight models were considered: (AI) Vertical adsorption of HCN gas on the boron site of pristine BPNTs *via* nitrogen head, (AII) Vertical adsorption of HCN gas on the boron site of Ga-doped BPNTs *via* nitrogen head, (AIII) Vertical adsorption of HCN gas on the boron site of N-doped BPNTs *via* nitrogen head, (AIV) Vertical adsorption of HCN gas on the boron site of GaN-doped BPNTs *via* nitrogen head, (BI) Vertical adsorption of HCN gas on the nitrogen site of pristine BPNTs *via* nitrogen head, (BII) Vertical adsorption of HCN gas on the nitrogen site of Ga-doped BPNTs *via* nitrogen head, (BIII) Vertical adsorption of HCN gas on the nitrogen site of N-doped BPNTs *via* nitrogen head and (BIV) Vertical adsorption of HCN gas on the nitrogen site of GaN-doped BPNTs *via* nitrogen head (See Fig. 1).

Subsequently, adsorption energy (E_{ads}) of HCN gas on the surface of pristine and Ga-, N- and GaN-doped BPNTs were calculated as follows:

$$E_{ads} = E_{BPNTs-HCN} - (E_{BPNTs} + E_{HCN}) \quad (1)$$

where $E_{BPNTs-HCN}$ is obtained from the scan of the potential energy of the BPNTs-HCN, E_{BPNTs} is the energy of the optimized BPNTs structure, and E_{HCN} is the energy of an optimized HCN. The quantum molecular descriptors electronic, chemical potential (μ), global hardness (η), electrophilicity index (ω), energy gap (E_{gap}), global softness (S) and electronegativity (χ) of the nanotubes were calculated as follows:

$$\mu = -(I + A)/2 \quad (2)$$

$$\eta = (I - A)/2 \quad (3)$$

$$\chi = -\mu \quad (4)$$

$$\omega = \mu^2/2\eta \quad (5)$$

$$S = 1/2\eta \quad (6)$$

$$E_{gap} = E_{LUMO} - E_{HOMO} \quad (7)$$

where I ($-E_{HOMO}$) is the ionization potential and A ($-E_{LUMO}$) the electron affinity of the molecule. The electrophilicity index is a measure of the electrophilicity power of a molecule [28-39]. The NQR parameters (the nuclear quadrupole coupling constants $C_{Q,}$ and the asymmetry parameter η_Q) are determined as above the level of theory. The NQR parameters refer to the interaction energy of the nuclear electric quadrupole moment and the EFG (Itensors at the site of quadrupole nucleus. Equations ((8), (9)) were used to convert the EFG tensors to the measurable parameters C_Q and η_Q [40]. The standard Q value of B atom is 40.59 *mb* [41].

$$C_Q\,(MHZ) = e^2 Q q_{zz} h^{-1} \quad (8)$$

$$\eta_Q = \left|(q_{xx} - q_{yy})/q_{zz}\right| \qquad (q_{zz} > q_{yy} > q_{xx}) \qquad 0 < \eta_Q < 1 \quad (9)$$

RESULTS AND DISCUSSION

Geometrical Parameters

To study the effects of Ga, N and GaN atoms, doped on the surface of BPNTs, on the adsorption of HCN gas, we consider eight stable configuration models, identified as AI, AII, AIII, AIV, BI, BII, BIII and BIV models, shown in

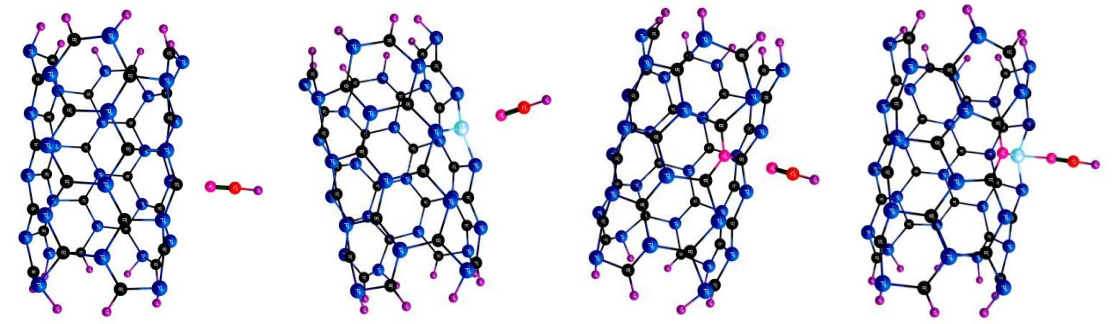

(AI) (AII) (AIII) (AIV)

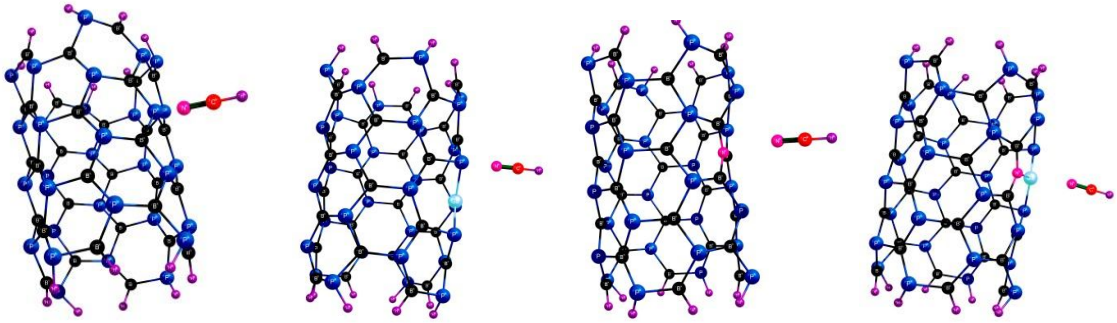

(BI) (BII) (BIII) (BIV)

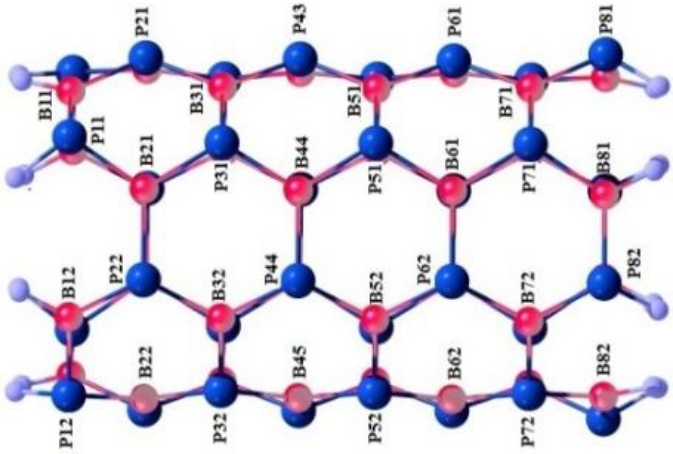

(P)

Fig. 1. 2D views of HCN adsorption on the surface of pristine, Ga, N and GaN-doped (4,4) armchair model of BPNTs for AI, AII, AIII, AIV, BI, BII, BIII and BIV models and (P) pure nanotube before adsorption (In all models blue color and black color identify phosphor and boron atom, respectively).

Fig. 1. The (A) type models show the vertical adsorption of HCN gas on the boron sites of nanotube and (B) type models indicate vertical adsorption of HCN gas on the nitrogen site of nanotube. The structural parameters involve the bond lengths of (B-P) and bond angles (B-P-B) of the pristine. Ga-, N- and GaN-doped of (4,4) armchair BPNTs are calculated and results are given in Table 1. The average B-P bond length of armchair forms of BPNTs is 1.89 Å, which is in agreement with other studies [20-23]. In (4,4) armchair BPNTs, by doping Ga on the B44 site, N on the P44 site and GaN on the B44 and P44 sites together, the bond lengths B-P increase from pristine values. With interaction of HCN gas on the surface of pristine, Ga-, N- and GaN-doped BPNTs the bond length B-P changes slightly from the original values. The bond angles of neighboring atoms of Ga- and N-doped in all models decrease from the original values. The radius of Ga is more than that of B atoms and therefore doping of Ga cause that the doped neighboring atoms are agglomerated and the bond angles are decreased.

The adsorption energy (E_{ads}) of HCN gas on the surface of BPNTs is calculated by Eq. (1) and results are given in Table 2 and are shown in Fig. 2. Figure 2 shows that the adsorption energy values of the AI-BIV models are negative and the adsorption process is exothermic. Comparing the results indicate that adsorption energy of the GaN-doped models (AIV and BIV) is more negative than that of other models. Therefore, GaN-doped impurity atoms increase the adsorption of HCN gas on the surface of nanotube and the GaN-doped models are more favorable than other models.

Tabe 1. Bond Length and Bond Angle Prameters of HCN Adorption on Pristine, Ga, N and GaN-doped of BPNTs (AI-BIV) Models, See Fig. 1

Bond Length (Å)								
properties	A(I)	A(II)	A(III)	A(IV)	B(I)	B(II)	B(III)	B(IV)
B44/Ga -P31	2.01	2.27	2.00	2.27	1.89	2.28	1.92	2.27
B44/Ga-P44/N	2.00	2.29	1.55	1.93	1.88	2.29	1.45	1.93
B32-P44/N	1.87	1.89	1.45	1.43	1.89	1.89	1.48	1.43
B44/Ga -P51	2.01	2.27	2.00	2.27	1.89	2.27	1.92	2.27
P44/N-B52	1.87	1.89	2.00	1.43	1.89	1.89	1.48	1.43
B32-P32	1.90	1.87	1.91	1.91	1.88	1.87	1.87	1.91
B52-P52	1.90	1.87	1.91	1.91	1.88	1.87	1.90	1.91
P31-B31	1.90	1.90	1.88	1.90	1.88	1.90	1.87	1.90
P51-B51	1.90	1.90	1.88	1.90	1.88	1.90	1.87	1.90
Bond Angle								
<P31-B44/Ga-N/P44	115.22	121.23	120.72	122.60	121.78	121.26	126.02	122.61
<B32-N/P44-B44/Ga	115.22	102.71	117.70	114.29	110.10	102.70	118.17	114.30
<B44/Ga-N/P44-B52	116.99	103.59	119.31	116.06	110.45	103.59	119.31	116.07
<P51-B44/Ga -N/P44	115.34	120.67	121.12	122.50	121.68	120.68	126.20	122.50
<P31-B44/Ga-P51	112.63	112.82	103.28	107.05	116.44	112.79	107.75	107.04
<B32-N/P44-B52	119.19	114.94	122.84	129.34	116.60	114.96	121.50	129.33
<B21-P31-B44/Ga	114.48	108.94	109.56	104.17	117.13	108.92	114.29	104.15
<B44/Ga -P51-B61	114.65	108.76	109.07	103.65	116.77	108.75	113.40	103.65
<P22-B32-N/P44	118.54	119.46	123.41	124.91	117.36	119.48	123.40	124.91
<N/P44-B52-P62	117.91	118.86	122.82	124.39	116.40	118.88	122.83	124.39

Table 2. The Quantum Molecular Descriptors Parameters of HCN Adorption on Pristine, Ga, N and GaN-doped of BPNTs the (AI-BIV Models, see Fig. 1), a (Pristine), b (Ga-doped), c (N-doped) and d (GaN-doped) before Adsorption HCN

Property	a	b	c	d	A(I)	A(II)	A(III)	A(IV)	B(I)	B(II)	B(III)	B(IV)
E (HOMO) (ev)	-5.94	-5.87	-5.86	-5.88	-5.51	-5.67	-5.67	-5.68	-5.77	-5.67	-5.75	-5.68
E (LUMO) (ev)	-2.76	-2.96	-2.88	-2.89	-2.67	-2.70	-2.67	-2.66	-2.81	-2.70	-2.77	-2.66
E_{FL}(ev)	-4.35	-4.41	-4.37	-4.38	-4.09	-4.18	-4.17	-4.17	-4.29	-4.18	-4.26	-4.17
I (ev)	5.94	5.87	5.86	5.88	5.51	5.67	5.67	5.68	5.77	5.67	5.75	5.68
A (ev)	2.76	2.96	2.88	2.89	2.67	2.70	2.67	2.66	2.81	2.70	2.77	2.66
μ (ev)	-4.35	-4.42	-4.37	-4.38	-4.09	-4.18	-4.17	-4.17	-4.29	-4.18	-4.26	-4.17
χ (ev)	4.35	4.42	4.37	4.38	4.09	4.18	4.17	4.17	4.29	4.18	4.26	4.17
η (ev)	1.59	1.45	1.48	1.49	1.41	1.48	1.50	1.51	1.48	1.48	1.48	1.51
S $(ev)^{-1}$	0.31	0.34	0.33	0.33	0.35	0.33	0.33	0.33	0.33	0.33	0.33	0.33
ω (ev)	5.94	6.71	6.43	6.44	5.90	5.90	5.81	5.75	6.23	5.90	6.11	5.75
ΔE (gap) (ev)	3.18	2.91	2.97	2.98	2.83	2.96	3.00	3.02	2.96	2.96	2.97	3.02
E_{ads} (kcal mol^{-1})	-	-	-	-	-14.3	-12.61	-1.38	-18.44	-14.90	-12.61	-2.13	-18.44
/NBOΔρ	-	-	-	-	0.283	0.141	0.293	0.152	0.004	0.141	0.014	0.151

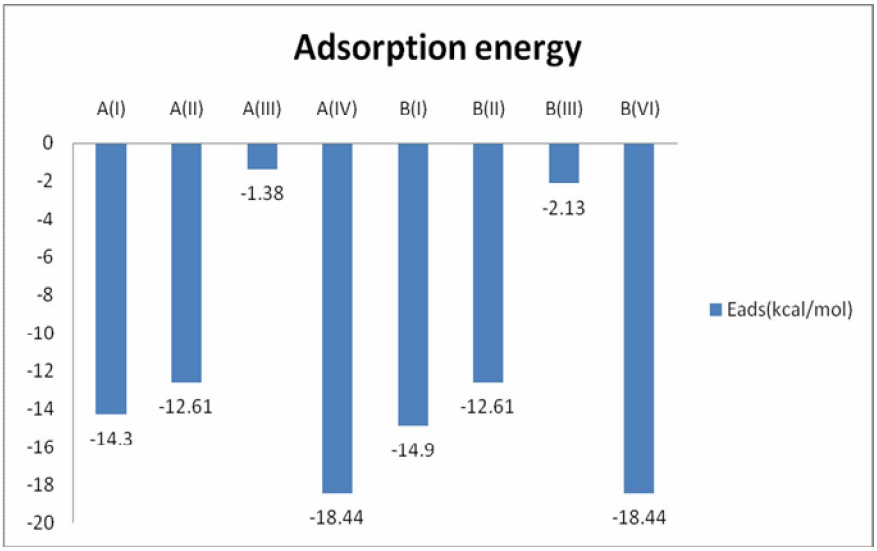

Fig. 2. Diagram of HCN adsorption energy on the surface of BPNTs for AI,AII, AIII, AIV, BI, BII, BIII and BIV models.

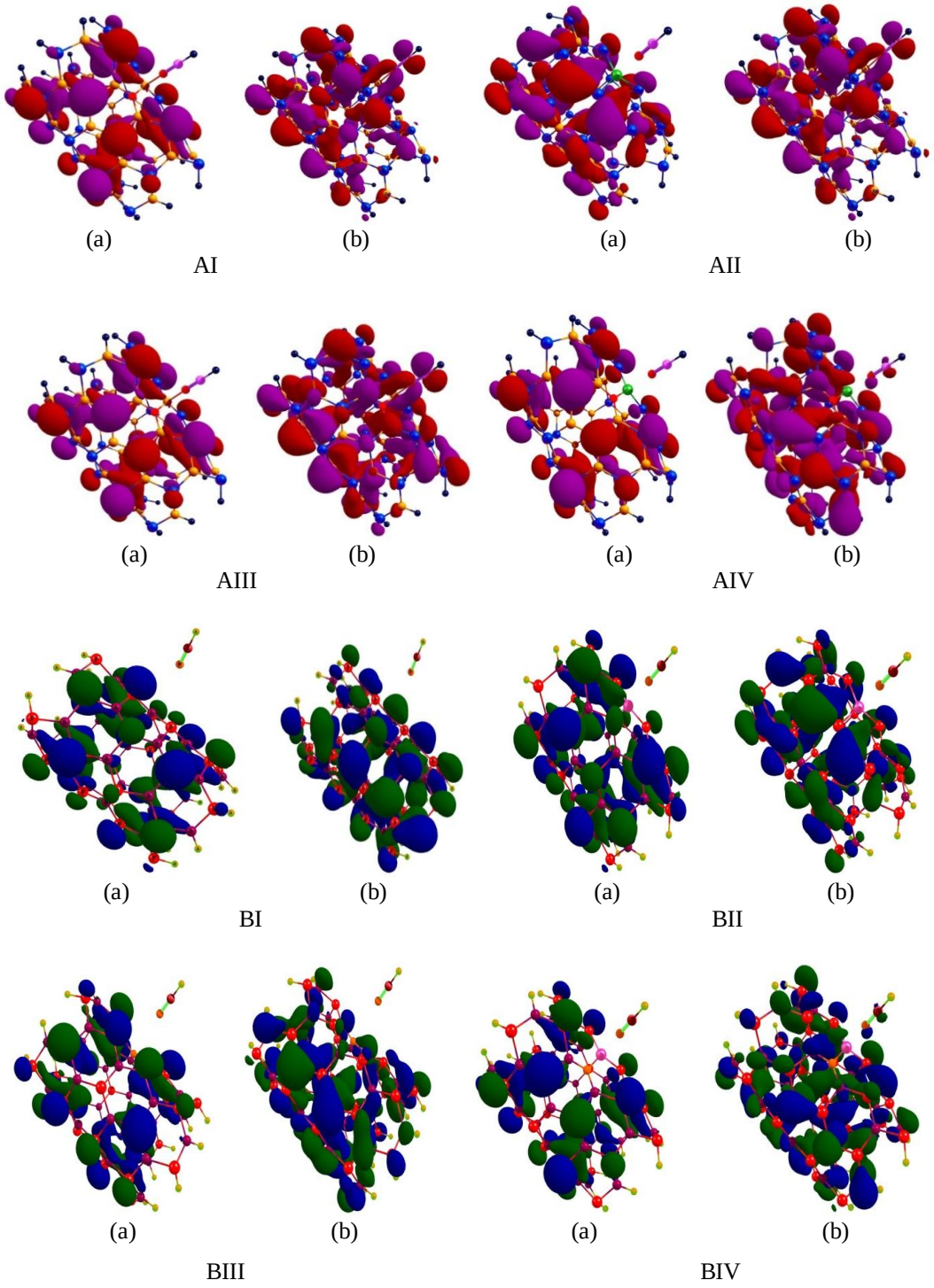

Fig. 3. Plots of HOMO and LUMO structures of HCN adsorption on the surface of BPNTs for AI, AII, AIII, AIV, BI, BII, BIII and BIV models, (a) and (b) index are used for HOMO and LUMO plots, respectively.

On the other hand, the adsorption energy of AIII and BIII models are lower than that of other models, due to weak Van der Waals interaction between the nanotube and the HCN molecule. Therefor, doping of N is not favourable for adsorption of HCN gas on the surface of BPNTs.

Quantum Molecular Descriptors

The highest occupied molecular orbital (HOMO) and lowest unoccupied molecular orbital (LUMO) on the AI, AII, AIII, AIV, BI, BII, BIII and BIV models are calculated by above level of theory and all structures are plotted in Fig. 3. Electron densities of HOMO and LUMO are uniformly distributed throughout the B-P bonds and neighbour of adsorption position. To study the electrical properties of HCN adsorption on the surface of pristine, Ga-, N-, GaN-doped of BPNTs at AI-BIV models, the quantum molecular descriptors are calculated and results are summarized in Table 2 and Figs. 4 and 6.

Figure 4 shows the comparison HOMO, LUMO and Fermi level energy for AI-BIV models. The energy level of HOMO is in the range -5.51 to -5.77 eV and the energy level of LUMO is in the range -2.66 to -2.77 eV. On the other hand, the Fermi energy level is in range -4.09 to -4.29 eV (see Fig. 4). The results reveal that the Fermi energy is closed to HOMO level orbital and it is expected to cause relatively large changes in the electrical conductivity of the semiconductor material that is favorable for sensor application. To gain a deeper understanding on the effect of HCN adsorption on the electronic properties of pristine, Ga-, N- and GaN-doped BPNTs, spectrum of the total density of states (DOS) for the most stable state of the pure nanotube and HCN/nanotube complex are calculated by using GaussSum package [42] and results are shown in Fig. 5. The DOS spectrum results reveal that all of the chemically modified BPNTs are still semiconductors with a wide E_{gap} close to that of the pristine BPNT and that the contribution of HCN is largely away from the Fermi level. However, upon the physical adsorption of HCN, E_{gap} of the BPNT is slightly changed from 2.96-3.02 eV. Comparing the DOS spectrum of a, b, c and d models of BPNTs before HCN adsorption and AI, AII, AII, AIV, BI, BII, BIII and BIV models of BPNTs after HCN adsorption show that the number of DOS peaks at the HOMO region are nine peaks and at the LUMO region are eight peaks. By doping Ga, N and GaN atoms the altitude of all pecks decrease significantly from pristine models, and so the photoelectric properties of all doped nanotube decrease from original form. In addition, the comparison of DOS spectrum before

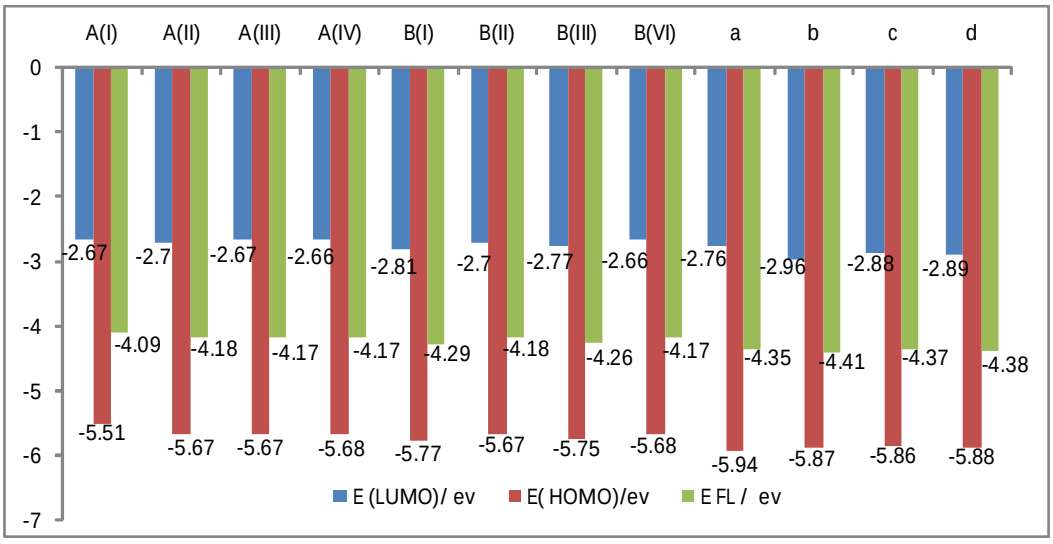

Fig. 4. Diagram of HOMO, LUMO and Fermi levels of HCN adsorption energy on the surface of BPNTs for AI, AII, AIII, AIV, BI, BII, BIII and BIV models.

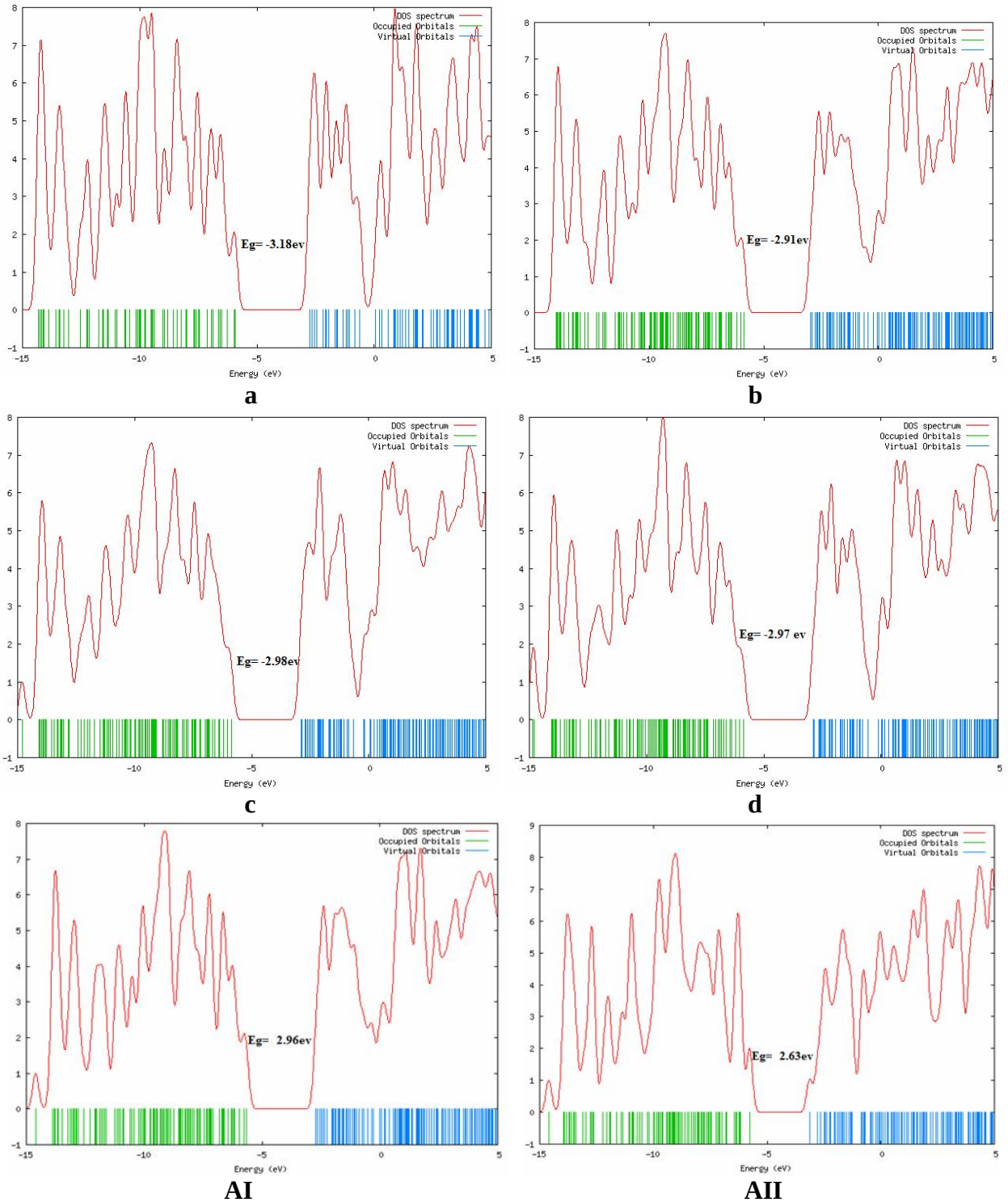

Fig. 5. Plots of DOS spectrum of HCN adsorption on the surface of BPNTs for AI, AII, AIII, AIV, BI, BII, BIII and BIV models, (a) model for pristine, (b) model for Ga-doped, (c) model for N-doped and (d) model for GaN-doped before HCN adsorption.

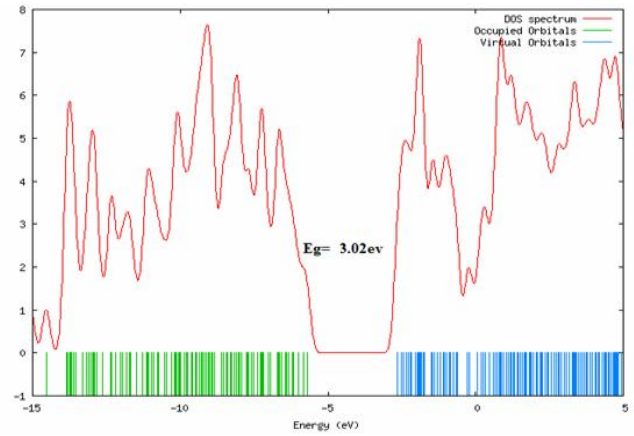

AIII

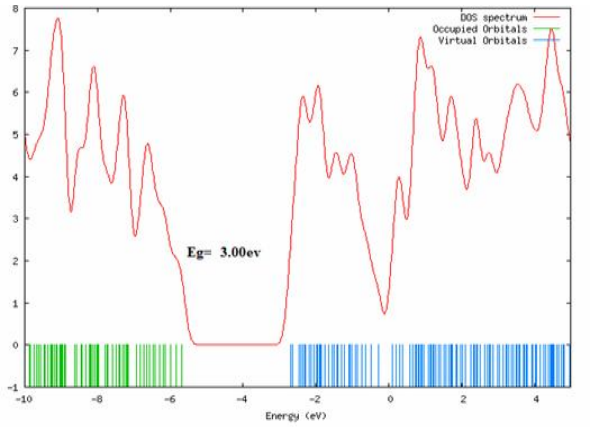

AIV

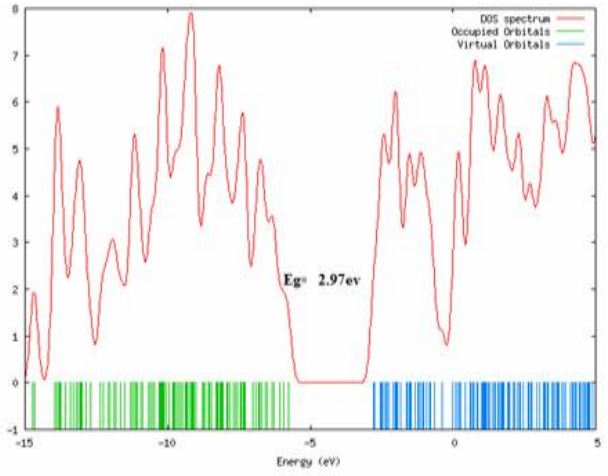

BI

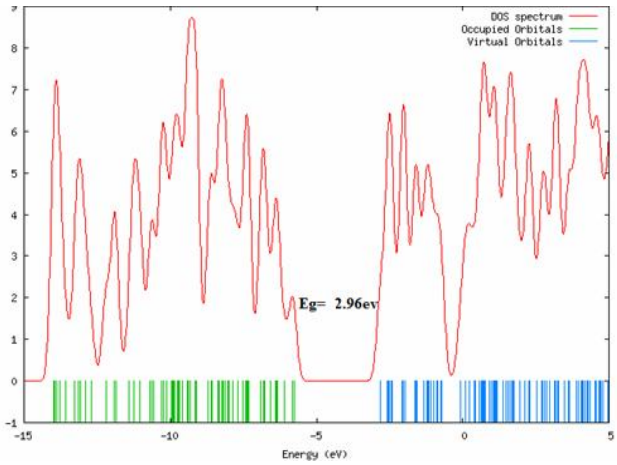

BII

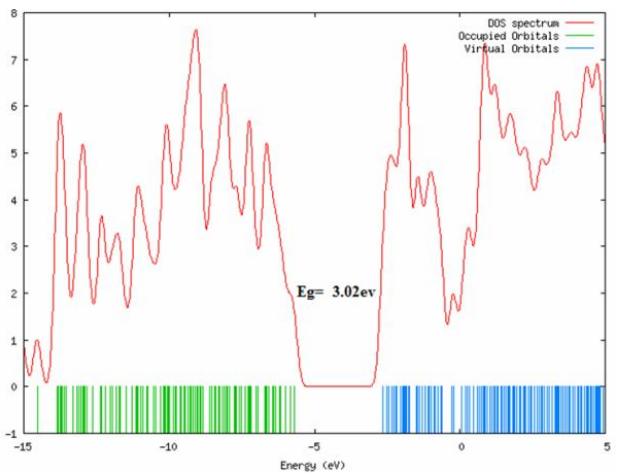

BIII

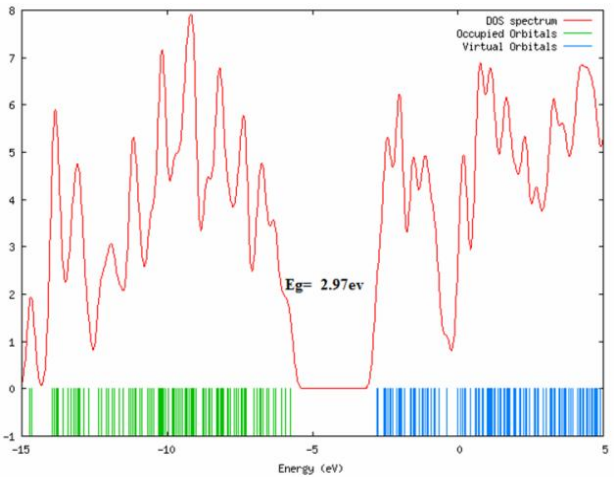

BIV

Fig. 5. Continued.

and after HCN adsorption show that the numbers of peaks are constant, the altitude of all peaks change slightly. In other words, comparing the results indicate that the interaction of HCN gas with BPNTs is rather weak, and that no significant hybridization of the respective orbitals of the two entities takes place; the small interaction is obtained quantitatively in terms of binding energies.

Figure 6 shows the energy gap (E_{gap}), electrophilicity index (ω), global hardness (η) for all adsorption models. The results reveal that the energy gap before HCN adsorption (models a, b, c and d) is in range 2.91-3.18 eV and with doping N, Ga and GaN atom the energy gap decreases slightly from original values. On the other hand, with adsorption HCN gas on the surface of BPNTs the energy gap changes from 2.83-3.09 eV. The energy gap of AI model is lower than that of other models and the energy gap of AIV and BIV models are more than that of other models. These changes of energy gap with HCN adsorption may be able to change the reactivity of the complexes, and show charge transfer between the HCN, Ga, N doped and the complexes sidewalls. Also, decrease in global hardness (η) and ionization potential with HCN adsorption shows a charge transfer from the HCN molecule (nucleophile agent) to the nanotube models (electrophile agent). The electrophilicity index (ω) is in range of 5.75-6.23 eV and the electrophilicity index of BI model is more than that of other models.

On the other hand, by using NBO analysis [43] the charge transfer between HCN gas and pristine, Ga-, N-, GaN-doped BPNTs (AI-BIV models) are calculated from the difference of the natural charge concentration ($\Delta\rho$) on HCN gas after adsorption and an isolated HCN. This calculation is performed by natural charge analysis of NBO, and results are given in Table 2 and are shown in Fig. 7. Looking at the results of Fig. 7 reveals that the $\Delta\rho_{(NBO)}$ values of AI-BIV models are positive and prove that HCN gas is electron donor and nanotube electron acceptor.

The calculated results of Table 2 reveal that the electronegativity (χ) parameters of AI-BIV models are reduced slightly from a-d models due to the HCN gas adsorption on the surface of BPNTs. The chemical potential (μ) values of BPNTs before and after adsorption of HCN gas are negative, structures of nanotube are stable, and with HCN adsorption, the μ values of AI-BIV models increase slightly from original values. Comparing the results show that the μ value of AI models is more than that of other models and this model is unstable than other models.

NQR Parameters of ^{11}B

The NQR parameters at various sites of ^{11}B nuclei for the optimized structures of AI-BIV models (Fig. 1) are calculated by using Eqs. (8) and (9) and the results are

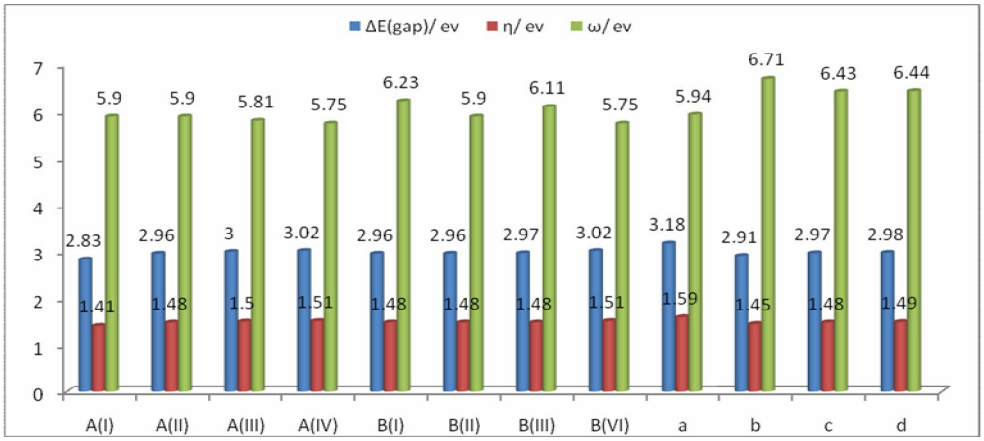

Fig. 6. Diagram of energy gap, global hardness (η), electrophilicity index (ω), fractional number of electrons transfered (ΔN) of HCN adsorption on the surface of BPNTs for AI, AII, AIII, AIV, BI, BII, BIII and BIV models.

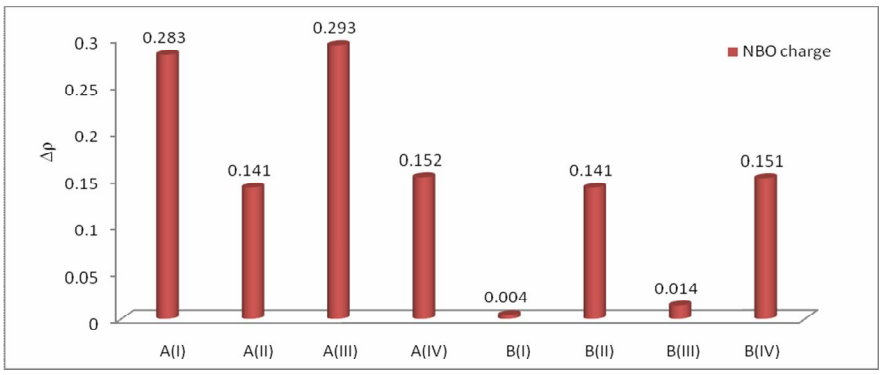

Fig. 7. Diagram of the difference of the natural charge concentration NBO (Δρ) of HCN gas after adsorption and an isolated HCN for AI, AII, AIII, AIV, BI, BII, BIII and BIV models.

Table 3. The NQR Parameters of HCN Adorption on Pristine, Ga, N and GaN-doped of BPNTs (AI-BIV) Models, See Fig. 1

B-11 nuclei	C_Q (MHZ)	η_Q	C_Q (MHZ)	η_Q	C_Q (MHZ)	η_Q	C_Q (MHZ)	η_Q
	A(I)		A(II)		A(III)		A(IV)	
Layer1	3.95	0.33	3.90	0.29	3.92	0.29	3.91	0.29
Layer2	2.49	0.07	2.58	0.07	2.58	0.07	2.61	0.07
Layer3	2.40	0.11	2.50	0.11	2.58	0.14	2.60	0.17
Layer4	2.06	0.05	1.71	0.04	2.18	0.07	1.81	0.06
	B(I)		B(II)		B(III)		B(IV)	
Layer1	3.93	0.30	3.91	0.29	3.92	0.29	3.91	0.28
Layer2	2.57	0.08	2.59	0.07	2.57	0.07	2.61	0.07
Layer3	2.51	0.11	2.50	0.11	2.58	0.12	2.60	0.16
Layer4	2.39	0.07	1.71	0.04	2.49	0.08	1.81	0.05

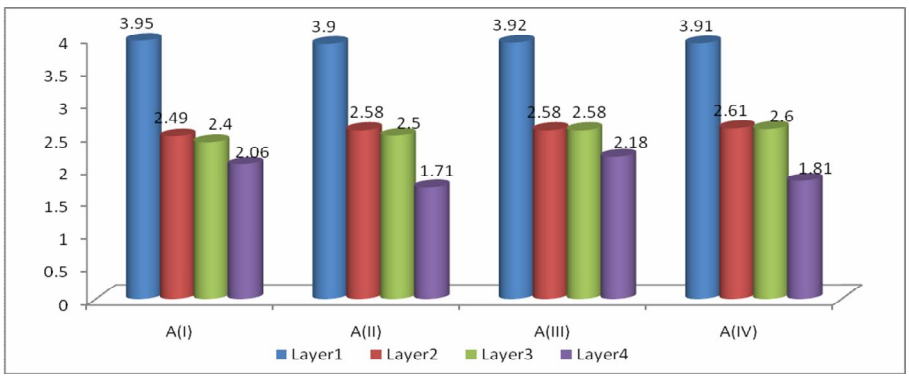

Fig. 8. Diagram of the nuclear quadrupole coupling constants C_Q of HCN adsorption on the surface of BPNTs for AI, AII, AIII, AIV, BI, BII, BIII and BIV models.

given in Table 3 and Fig. 8.

Figure 8 indicates the variation of quadrupole tensor (C_Q) for layers 1 to 4 for all adsorption models. Comparing the results reveal that the NQR parameters of 32 B atoms in all considered adsorption (AI-BIV) models are separated into four layers based on the similarity of the calculated electric field gradient (EFG) tensors in each layer; therefore, the electrostatic environment of the BPNTs is equivalent along each layer. The comparison of C_Q values show that the first layers of all models have the largest among other layers. The results show that the orientation of the EFG tensor eigenvalues along the Z-axis of the first layer is stronger than that of the other layers along the length of the nanotube. On the other hand, the fourth layer has the low C_Q value among other layers in alone nanotube. The significant difference between NQR parameters in the first layer and the fourth layer is due to the change of the geometrical parameters. The C_Q values of the first, second and third layers with adsorption of HCN at all models are almost constant. On the other hand, the C_Q values of the fourth layer of pristine models (AI and BI) and N-doped models (AIII and BIII) are more than those of other models due to the change of the geometrical parameters. The asymmetry parameter (η_Q) values of the first layers of all models are more than those of other layers and the forth layers are lower than other layers. Comparing the results show that the η_Q values for (AI-BIV) models at all layers are changed slightly.

CONCLUSIONS

In this work, we study the adsorption of HCN gas on surface of pristine, Ga-, N- and GaN-doped of BPNTs by using DFT theory. The geometrical results show that with adsorption HCN gas on the surface of pristine and Ga-, N- and GaN-doped BPNTs, the bond length and bond angles change slightly from the original values. The adsorption energy values of all models are negative and the adsorption process is exothermic. Comparing the results reveal that the adsorption energy of AIV and BIV models are more negative than that of other models. Therefore, GaN-doped impurity atoms increase the adsorption of HCN on the surface of nanotube and the GaN-doped models are more favorable than other models. On the other hand, the adsorption energy of AIII and BIII models are lower than that of other models. We observe that the energy gap of AI model is lower than that of other models and the energy gap of AIV and BIV models is more than that of other models. These changes of energy gap with HCN adsorption may be able to change the reactivity of the complexes, and show charge transfer between the HCN, Ga, N and GaN-doped and the complexes sidewalls.

The analysis of natural charge from NBO calculations prove that HCN gas is electron donor and nanotube is electron acceptor. The C_Q values of the fourth layer of AI, BI, AIII and BIII models are more than those of other models due to the change of the geometrical parameters.

ACKNOWLEDGMENTS

The authors thank the Centre of computational nano of Malayer Universities for supporting this research.

REFERENCES

[1] T. Blank, M. Roloff, R. Short, S. Schuengel, W. Ribelin, Toxicol. Lett. 18 (1983) 136.

[2] B. Akyildiz, S. Kurtoğlu, M. Kondolot, A. Tunç, Annals of Tropical Paediatrics: International Child Health, 30 (2010) 39.

[3] W.H. Organization, Concise International Chemical Assessment Document 61 (2004).

[4] J. Risher, G. Diamond, S. Swarts, R. Amata, in, US Department of Health and Human Services; Toxicological Profile for Iodine, 2004.

[5] B. Mégarbane, A. Delahaye, D. Goldgran-Tolédano, F.J. Baud, J. Chin. Med. Assoc. 66 (2003) 193.

[6] A.E. Lindsay, A.R. Greenbaum, D. O'Hare, Anal. Chim. Acta 511 (2004) 185.

[7] F.J. Baud, P. Barriot, V. Toffis, B. Riou, E. Vicaut, Y. Lecarpentier, R. Bourdon, A. Astier, C. Bismuth, New Engl. J. Med. 325 (1991) 1761.

[8] D.J. Barillo, R. Goode, V. Eseh, J. Burn. Care Res. 15 (1994) 46-57.

[9] K.S. Brown, R.R. Robinette, Nature 215 (1967) 406.

[10] A. Allison, Man 53 (1953) 176.

[11] P. Parthangal, R.E. Cavicchi, D.C. Meier, A. Herzing, M.R. Zachariah, J. Mater. Res. 26 (2011)

430.

[12] P. Qi, O. Vermesh, M. Grecu, A. Javey, Q. Wang, H. Dai, S. Peng, K. Cho, Nano lett. 3 (2003) 347.

[13] M. Zhao, F. Yang, Y. Xue, D. Xiao, Y. Guo, J. Mol. Model. 20 (2014) 1.

[14] Y. Zhang, Y. Zhang, D. Zhang, C. Liu, J. Phys. Chem. B 110 (2006) 4671.

[15] X. Zhou, W.Q. Tian, The J. Phys. Chem. C 115 (2011) 11493.

[16] R. Wang, D. Zhang, Y. Liu, C. Liu, Nanotechnology 20 (2009) 505704.

[17] S.F. Rastegar, A.A. Peyghan, N.L. Hadipour, Appl. Surf. Sci. 265 (2013) 412.

[18] A. Ahmadi Peyghan, N.L. Hadipour, Z. Bagheri, J. Phys. Chem. C 117 (2013) 2427.

[19] J. Beheshtian, A.A. Peyghan, Z. Bagheri, Comput. Mater. Sci. 62 (2012) 71.

[20] M.T. Baei, Comput. Theoretical Chem. 1024 (2013) 28.

[21] R. Wu, M. Yang, Y. Lu, Y. Feng, Z. Huang, Q. Wu, The J. Phys. Chem. C 112 (2008) 15985.

[22] S. Zhang, Phys. Lett. A 285 (2001) 207.

[23] M. Rezaei-Sameti, Physica E: Low-dimensional Systems and Nanostructures 43 (2010) 588.

[24] M. Rezaei-Sameti, Physica B: Condensed Matter 407 (2012) 3717.

[25] M. Rezaei-Sameti, Physica B: Condensed Matter 407 (2012) 22.

[26] M. Rezaei-Sameti, Physica E: Low-dimensional Systems and Nanostructures 44 (2012) 1770.

[27] A. Frisch, M.J. Frisch, Gaussian 03 Pocket Reference, Gaussian, Incorporated, 2003.

[28] R. Ditchfield, W.J. Hehre, J.A. Pople, J. Chem. Phys. 54 (1971) 724.

[29] M.T. Baei, M. Moghimi, P. Torabi, A.V. Moradi, Comput. Theoretical Chem. 972 (2011) 149.

[30] P.K. Chattaraj, U. Sarkar, D.R. Roy, Chem. Rev. 106 (2006) 2065.

[31] K.K. Hazarika, N.C. Baruah, R.C. Deka, Struct. Chem. 20 (2009) 1079.

[32] R.G. Parr, L.v. Szentpaly, S. Liu, J. Am. Chem. Soc. 121 (1999) 1922.

[33] R.G. Pearson, J. Chem. Sci.-B 117 (2005) 369.

[34] T. Koopmans, Physica 1 (1933) 104.

[35] R.G. Pearson, J. Am. Chem. Soc. 85 (1963) 3533.

[36] R.G. Parr, R.G. Pearson, J. Am. Chem. Soc. 105 (1983) 7512.

[37] P. Politzer, J.S. Murray, F.A. Bulat, J. Mol. Model. 16 (2010) 1731.

[38] R.S. Mulliken, J. Chem. Phys. 2 (1934) 782.

[39] C. Tabtimsai, S. Keawwangchai, N. Nunthaboot, V. Ruangpornvisuti, B. Wanno, J. Mol. Model. 18 (2012) 3941.

[40] B.C. Gerstein, C.R. Dybowski (1985).

[41] P. Pyykkö, Mol. Phys. 99 (2001) 1617.

[42] N.M. O'boyle, A.L. Tenderholt, K.M. Langner, J. Comput. Chem. 29 (2008) 839.

[43] A.E. Reed, L.A. Curtiss, F. Weinhold, Chem. Rev. 88 (1988) 899.